Inter-Numerology Interference Analysis and Cancellation for Massive MIMO-OFDM Downlink Systems

Xinying Cheng, Rafik Zayani, Hmaied Shaiek, Daniel Roviras

IEEE Access
Multidisciplinary | Rapid Review | Open Access Journal

Received October 24, 2019, accepted November 9, 2019, date of publication December 2, 2019, date of current version December 23, 2019.

Digital Object Identifier 10.1109/ACCESS.2019.2957194

Inter-Numerology Interference Analysis and Cancellation for Massive MIMO-OFDM Downlink Systems

XINYING CHENG[1], (Student Member, IEEE), RAFIK ZAYANI[2], (Member, IEEE), HMAIED SHAIEK[1], (Member, IEEE), AND DANIEL ROVIRAS[1], (Senior Member, IEEE)

[1]CEDRIC/LAETITIA, CNAM, 75003 Paris, France
[2]LR-11/TIC-03 Innov'COM Laboratory, Higher School of Communication of Tunis, University of Carthage, Ariana 2083, Tunisia

Corresponding author: Xinying Cheng (xinying_cheng@126.com)

This work was supported in part by the framework of the ADAM5 Project receiving fund by the European Union under H2020-EU.1.3.2 with funding scheme MSCA-IF-EF-ST under Project 796401, and in part by the Scholarship of Sorbonne Université, Paris, France.

ABSTRACT The extremely diverse service requirements is an important challenge for the upcoming fifth-generation (5G) wireless communication technologies. Orthogonal frequency division multiplexing (OFDM)-based massive multiple-input multiple-output (MIMO) and mixed numerologies transmission are proposed as solutions. This paper investigates the use of spatial multiplexing of users, sharing the same bandwidth, whose associated numerologies are different. We first introduce a precoding design that aims to manage the mixed numerologies spectrum sharing (SS) transmission. Then, we analyse the inter-numerology interference (INI) and derive the theoretical expressions of its radiation pattern in massive MIMO-OFDM downlink systems. We demonstrate that by using the proposed precoding scheme and considering two groups of users using two different numerologies, INI appears only in frequency selective channels. Besides, the transmission of users using numerology with large subcarrier spacing (SCS) is always with the best quality, only users using the numerology with small SCS suffer from INI. In that case, INI increases due to the difference in SCS, channel selectivity and power allocation. Based on the derived INI, in closed-form expressions, the precoding scheme is improved and a new INI cancellation scheme is introduced. Our analysis demonstrates that the INI theoretical model matches the simulation results, and the introduced INI cancellation based precoder efficiently mitigates the INI and enhances the performance of massive MIMO-OFDM downlink systems.

INDEX TERMS Massive MIMO-OFDM, mixed numerologies, spectrum sharing (SS), 5G.

I. INTRODUCTION

The upcoming 5G wireless communication system is expected to support a wide range of services with diverse requirements. Multiple-input multiple-output (MIMO) technology was established and developed as it meets the demand by offering increased spectral efficiency through spacial multiplexing gain and improved link reliability through antenna diversity gain. Reference [1] gives an overview of MIMO communications. Recently, researchers have shown an increased interest in massive MIMO technology which is recognized as a key feature for the evolution of future communication systems [2]. The concept was first presented in [3] with the name of massive multi-user (MU) MIMO system in which the base station (BS), equipped with a large number of antennas, serves simultaneously several single-antenna users [4]. The number of users are much smaller than the number of antennas in the BS and all the users share the multiplexing gain so that spectral and energy efficiency is improved [5]–[7]. Furthermore, precoding techniques can be used at the BS to suppress multi-user interference (MUI) and reduce the power consumption [8].

Wireless communication suffers from frequency-selective fading in practice. Orthogonal frequency division multiplexing (OFDM) which uses multiple orthogonal subcarriers, is an efficient and widely-used technique to deal with

The associate editor coordinating the review of this manuscript and approving it for publication was Jules Merlin Moualeu.

frequency-selective channels [9]. In addition, OFDM will most likely remains as the base technology of 5G [10]. Therefore, massive MIMO-OFDM is a very promising combination to meet the ever growing demands for higher spectral efficiency in next-generation wireless communication system [11].

Another step which brings more flexibility in the communication system is the mixed numerologies proposed in 5G New Radio (NR) [12]. The different service requirements can be categorized into three main scenarios: enhanced mobile broadband (eMBB), massive machine type communications (mMTC), and ultra-reliable and low latency communications (URLLC) [13]. In particular, mMTC and URLLC require critical capability objectives such as 10^6 devices/km^2 connection density, ultra high energy efficiency, low cost terminals, 1 ms latency and mobility up to 500 km/h [14], presenting serious challenges on 5G commercial deployments. Hence, mixed numerologies systems are being proposed where the numerology varies based on the requirement of the service characteristics. Different numerologies refer to different parameters setting in OFDM such as subcarrier spacing (SCS), symbol duration and cyclic prefix (CP) length. One of the first studies which introduced the multi-numerology or mixed numerologies system is [15]. Mixed numerologies structures are also included in the Third Generation Partnership Project (3GPP) NR standardization and are studied in many papers [14], [16]–[19]. From the above works, the most accepted way proposed to support diverse services is to divide the bandwidth into several subband, then flexible allocation of different numerologies are implemented in each subband. Although, the usage of numerology multiplexing significantly improves the system flexibility, the interference between users belonging to different numerologies appears and the inter-numerology interference (INI) affects the system performance.

An INI model is built, in [20] as a function of spatial spacing between numerologies, overlapping windows and channel frequency response. Although this work establishes theoretical expressions, this model is limited to single-input single-output (SISO) Windowed-OFDM system and to the users occupying adjacent subbands. Factors that affect INI in a mixed numerologies OFDM system are discussed in [21], which investigated the INI problems and explained its underlying causes such as SCS, number of activated subcarriers, power, etc. However, this work is still limited to SISO systems with adjacent bands and only simulation results were presented. Also, [22] gives the similar results as the two above papers, where the INI occurs near the junction of the two subbands. Recently, some works [23], [24] have dealt with mixed numerologies spectrum sharing (SS), which can be also described as overlapping mixed numerologies. Unlike in non-overlapping mixed numerologies system, in mixed numerologies SS systems (i.e., users are sharing the same time/frequency resources), it is impossible to avoid interference using windowed/filtered waveforms. In [24], authors introduced a new transceiver design considering a mixed numerologies SS system for classical MIMO-OFDM, where the users have different SCS. Derivation of the interference pattern is given but again, no theoretical model is proposed and only the simulation results are shown.

In massive MIMO-OFDM systems, it is desirable to assign the full bandwidth to all users in order to guarantee high spectral efficiency while satisfying the flexible services. It is worth noticing that this SS system is different from the SISO/classical MIMO case where adjacent bandwidths, separated by a guard band, are assigned to different users, where INI exists at the two edges of the subbands [18], [19]. Also, unlike the SISO/classical MIMO system with different numerologies, in a massive MIMO system, MUI contains two parts: Intra-Numerology Interference (Intra-NI) and INI, where the former indicates the interference between users within the same numerology and the latter indicates the interference between users using different numerologies. Using the high dimensional degrees of freedom (DoFs), the Intra-NI is cancelled by precoders due to the numerous transceiver antennas. Unlike the classical MIMO, in massive MIMO, some hypothesis can be added to simplify the computation of an analytical model for the INI with great accuracy. What is more, we can improve the transceiver design proposed for classical MIMO in order to enhance the INI management and cancellation. To the best of our knowledge, no general analysis and analytical expressions of the INI have been presented for massive MIMO-OFDM in the open literature. In addition, it is still not yet clear how MU massive MIMO-OFDM systems perform in mixed numerologies SS transmission. Besides, the MU precoder design and analysis, efficient INI cancellation algorithm are needed to achieve good performance. We will study, for the first time, the INI impact and its cancellation for the Massive MIMO-OFDM, which have great difference to the ever proposed SISO and classical MIMO systems. Regarding the previous works and motivations behind this work, the main contributions of this paper are:

- An improved transceiver scheme is introduced for massive MIMO-OFDM downlink system to enable flexible management of mixed numerologies SS transmission. It is similar to the one proposed in [23] but we adopt a different precoding branch and a different zero-adding process for each numerology. Then, the time-domain superposition of all signals maximize the spectrum efficiency but introduce INI on certain users. The INI is analysed regarding many patterns such as SCS, channel selectivity and power allocation.
- A analytical INI model is built for massive MIMO-OFDM system with mixed numerologies, which could be a good tool to guide 5G system design and parameters selection. We derive the theoretical INI expressions in closed-form to analyse theoretically the impact of INI on the users' performance. Theoretical results match the simulation ones, confirming our theoretical study.
- Based on the derived theoretical expressions of INI between different numerologies, we investigate an INI

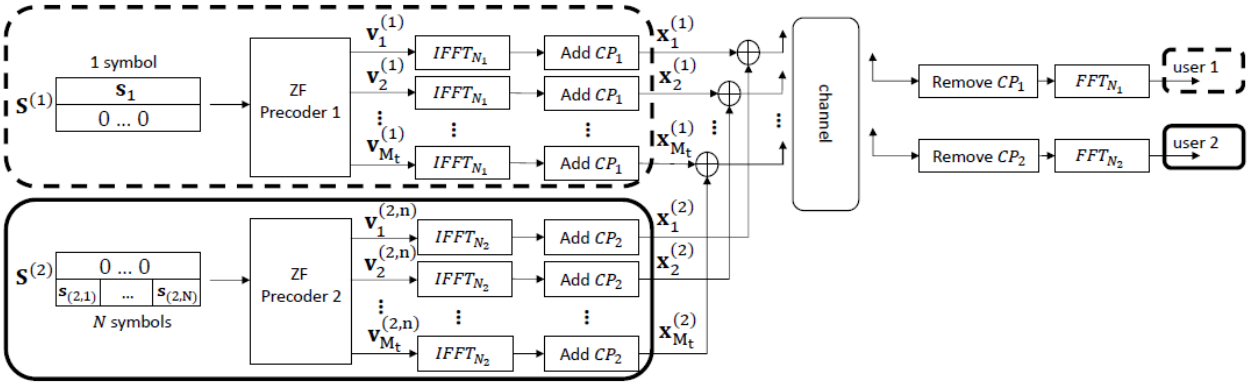

FIGURE 1. System model of the massive MIMO OFDM downlink with two different numerologies: M_t transmit antennas at the BS, two sigle-antenna terminals, two blocks illustrate two different numerologies with OFDM of N_1 and N_2 subcarriers.

cancellation method. The cancellation is implemented only at the BS side so that no more complexity is added at the receiver side.

The rest of this paper is structured as follows. Section II presents the system model investigated in this study. Section III analyses the INI between different numerologies and gives the theoretical INI expressions. Section IV introduces the INI cancellation based on the previous analysis. Simulation results are provided in section V. Finally, the conclusion is given in section VI.

Notations: Lower-case letters (e.g. x), bold lower-case letters (e.g. $\mathbf{x}$), bold upper-case letters (e.g. $\mathbf{X}$) stand for scalars, vectors and matrices, respectively. $\bar{\mathbf{H}}$ denotes a $M \times N \times K$ 3-dimension matrix. We denote the trace, transpose, conjugate transpose and pseudo-inverse by $tr(\mathbf{X})$, $\mathbf{X}^T$, $\mathbf{X}^H$ and $\mathbf{X}^\dagger$, respectively. The superscript represent the numerology index (e.g. $\mathbf{X}^{(1)}$). The k-th element in the vector $\mathbf{x}$ is denoted as $\mathbf{x}[k]$. For a $M \times N$ matrix $\mathbf{X}$, $\mathbf{X}(m, :)$ denote the m-th line and $\mathbf{X}(:, n)$ denote the n-th column. $N \times N$ identity matrix, $M \times N$ all-zeros matrix, $N \times N$ discrete Fourier transform (DFT) matrix and $N \times N$ inverse discrete Fourier transform (IDFT) matrix are denoted by $\mathbf{I}_N$, $\mathbf{0}_{M\times N}$, $\mathbf{DFT}_N$ and $\mathbf{IDFT}_N$, respectively. $Diag(\mathbf{x})$ represents the matrix where the diagonal elements are vector $\mathbf{x}$ and all off-diagonal elements are zero. We use $\| \mathbf{x} \|^2$ to denote l_2-norm of vector $\mathbf{x}$. $\mathbb{E}\{.\}$ and $\lceil x \rceil$ stand for the expectation operator and the ceiling function, respectively.

II. SYSTEM MODEL

We consider, in this paper, a massive MIMO-OFDM downlink system with different numerologies. The BS is equipped with M_t antennas serving M_r single-antenna users that use different numerologies over a frequency-selective channel, where M_t is significantly larger than M_r. The M_r users can be divided into NUM groups using NUM numerologies, represented by index num, where $num = 1, \ldots, NUM$. N_{num} and CP_{num} denote the IFFT/FFT size and CP size of group num, respectively. The transceiver design is different to the one introduced in [23], where we add zeros in each users' signal structure to allow flexible INI managements. In this way, our transceiver permits the suppression of Intra-NI by using several precoders and the added zeros help the implementation of INI cancellation, which will be discussed later. The BS transmits, via the m_t-th antenna, to the m_r-th user over channel $\sqrt{\alpha_{m_r}}\mathbf{ht}_{m_r,m_t}$, where α_{m_r} is the large-scale fading, $\mathbf{ht}_{m_r,m_t} \in \mathbb{C}^{1\times D}$ is the channel impulse response between transmitting antenna m_t and user m_r, $m_t = 1 \ldots M_t$, $m_r = 1 \ldots M_r$ and D is the number of taps.

Then,

$$\mathbf{hf}^{(num)}_{m_r,m_t} = FFT(\sqrt{\alpha_{m_r}}\mathbf{ht}_{m_r,m_t}, N_{num}). \quad (1)$$

is the channel frequency response with FFT size N_{num}. For a massive MIMO-OFDM system, the channel frequency response is denoted by $\bar{\mathbf{H}}^{(num)} \in \mathbb{C}^{M_r\times M_t\times N_{num}}$, where

$$\bar{\mathbf{H}}^{(num)}(m_r, m_t, :) = \mathbf{hf}^{(num)}_{m_r,m_t}. \quad (2)$$

The construction of $\bar{\mathbf{H}}^{num}$ is presented on Fig. 2.

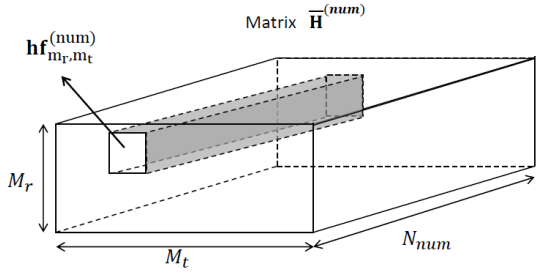

FIGURE 2. Structure of matrix $\bar{\mathbf{H}}^{num}$.

In order to simplify the system without loss of generality, we consider, in this paper, two users ($M_r = 2$) using two different numerologies, as shown in Fig. 1. $\mathbf{s}_1, \mathbf{s}_2 \in \mathbb{C}^{1\times N_1}$ are signals generated by M-quadrature amplitude modulation (QAM) for user 1 and user 2, respectively. Synchronization is achieved over the least common multiplier (LCM) methods [24] which is illustrated in Fig. 3. Considering this generalized synchronized scenario, which is also considered in previous works [17], [20], we assume that $N_1 = N \times N_2$,

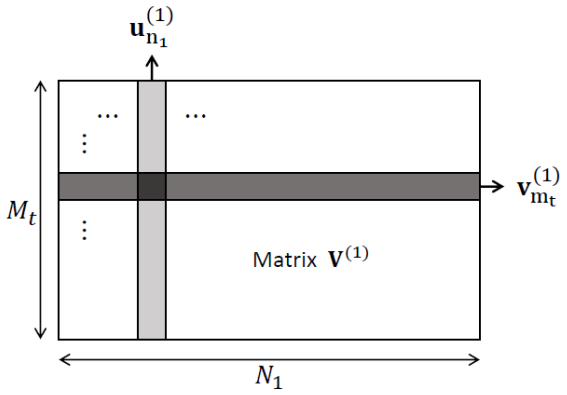

FIGURE 3. Signal synchronization and summation. $\mathbf{x}_{m_t}^{(1)}$ is user 1's signal on *mt*-th transmitting antenna, $\mathbf{x}_{m_t}^{(2)}$ is user 2's signal on *mt*-th transmitting antenna.

$CP_1 = N \times CP_2$, where $N = 2^i$ and i is an integer. $\mathbf{x}_{m_t}^{(1)}$ is user 1's OFDM-modulated symbol on m_t-th transmitting antenna and $\mathbf{x}_{m_t}^{(2,n)}$ is user 2's n-th OFDM-modulated symbol on m_t-th transmitting antenna. The total symbol length of $\mathbf{x}^{(1)}$ is N times the symbol length of $\mathbf{x}^{(2,n)}$ and all the symbols are aligned.

In order to suppress the Intra-NI at the receivers, linear precoding scheme is implemented at the BS. In order to enable flexible management, we consider two linear precoding branches, each for one numerology, at the BS, where two zero-forcing (ZF) precoders are used [25]. Looking at branch one (dash-line block) in Fig. 1, the first line of matrix $\mathbf{S}^{(1)}$ is the data information vector $\mathbf{s}^{(1)}$ in numerology 1 for user 1, while the second line is set to zero aiming to protect user 2. One can also note that in the second branch (solid-line block), matrix $\mathbf{S}^{(2)}$ contains data vector $\mathbf{s}^{(2)}$ for user 2 and null-vector is prepared for user 1.

Then, ZF precoding is performed at each branch, which is designed to cancel the Intra-NI between users within the same group completely. Thus, the signal matrices $\mathbf{S}^{(1)}, \mathbf{S}^{(2)} \in \mathbb{C}^{2\times N_1}$ are linearly coded as

$$\mathbf{u}_{n_1}^{(1)} = \frac{1}{\sqrt{\zeta_{n_1}^{(1)}}}\mathbf{P}_{n_1}^{(1)}\mathbf{s}_{n_1}^{(1)}, \quad n_1 = 1, \ldots, N_1, \tag{3}$$

$$\mathbf{u}_{n_2}^{(2,n)} = \frac{1}{\sqrt{\zeta_{n_2}^{(2,n)}}}\mathbf{P}_{n_2}^{(2)}\mathbf{s}_{n_2}^{(2,n)}, \quad n_2 = 1, \ldots, N_2 \,\&\, n = 1, \ldots N. \tag{4}$$

where $\zeta_{n_1}^{(1)}$, $\zeta_{n_2}^{(2,n)}$ are power normalization factors, $\mathbf{P}_{n_{num}}^{(num)} \in \mathbb{C}^{M_t\times M_r}$ denotes the ZF precoding matrices for n_{num}-th OFDM subcarrier of numerology *num*. $\mathbf{s}_{n1}^{(1)} = \mathbf{S}^{(1)}(:, n_1) \in \mathbb{C}^{2\times 1}$, $\mathbf{u}_{n1}^{(1)} \in \mathbb{C}^{M_t\times 1}$ are the original signal on the n_1-th subcarrier and the precoded vectors of the n_1-th subcarrier with numerology 1, $\mathbf{s}_{n_2}^{(2,n)} = \mathbf{S}^{(2)}(:, n_2 + (n-1)\cdot N_2) \in \mathbb{C}^{2\times 1}$, $\mathbf{u}_{n_2}^{(2,n)} \in \mathbb{C}^{M_t\times 1}$ are the original signal of the n_2-th subcarrier for n-th symbol and the precoded vector of the n_2-th subcarrier for n-th symbol with numerology 2. The ZF precoding matrices are

$$\mathbf{P}_{n_{num}}^{(num)} = \mathbf{H}_{n_{num}}^{(num)H}\left(\mathbf{H}_{n_{num}}^{(num)}\mathbf{H}_{n_{num}}^{(num)H}\right)^{-1} \tag{5}$$

where $\mathbf{H}_{n_{num}}^{(num)} = \bar{\mathbf{H}}^{(num)}(:, :, n_{num}) \in \mathbb{C}^{2\times M_t}$ is the MIMO channel frequency response of the n_{num}-th OFDM subcarrier with numerology *num*. We assume that channel matrices are perfectly known at the BS, which can be determined by exploiting the channel reciprocity of time division multiplexing (TDD) systems [26], [27].

After precoding, the M_t-dimension vector $\mathbf{u}_{n_1}^{(1)}$ and $\mathbf{u}_{n_2}^{(2,n)}$ are reordered to construct matrices $\mathbf{V}^{(1)}$ and $\mathbf{V}^{(2,n)}$, according to the following mapping:

$$\mathbf{v}_{m_t}^{(1)} = \left[\mathbf{u}_1^{(1)}[m_t] \ldots \mathbf{u}_{N_1}^{(1)}[m_t]\right], \tag{6}$$

$$\mathbf{v}_{m_t}^{(2,n)} = \left[\mathbf{u}_1^{(2,n)}[m_t] \ldots \mathbf{u}_{N_2}^{(2,n)}[m_t]\right]. \tag{7}$$

where $\mathbf{v}_{m_t}^{(1)} \in \mathbb{C}^{1\times N_1}$ and $\mathbf{v}_{m_t}^{(2,n)} \in \mathbb{C}^{1\times N_2}$ are each line of the precoded signals. Fig. 4 gives the structure of matrix $\mathbf{V}^{(1)}$ and the matrix $\mathbf{V}^{(2,n)}$ is constructed similarly. Then, the time-domain signals are obtained by applying IFFTs and adding CPs. Before transmission over wireless channel, the signals of two different numerologies are added point by point for each transmitting antenna. Fig. 3 also shows the adding process at each transmit antenna m_t. It is worth noticing that in the proposed system, users share the same bandwidth, which provides a high spectrum efficiency. At the receiver side, assuming that the length of CP_{num} is larger than the length of the multipath channel, then inter-symbol interference (ISI) are eliminated.

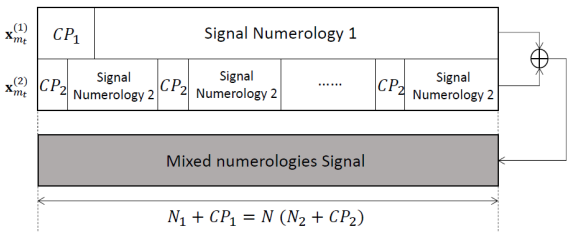

FIGURE 4. Structure of matrix $\mathbf{V}^{(1)}$.

Since $\mathbf{H}_{n_{num}}^{(num)}\left(\mathbf{H}_{n_{num}}^{(num)}\right)^{\dagger} = \mathbf{I}_{Mr}$, transmitting $\mathbf{u}_{n_{num}}^{(num)} = \left(\mathbf{H}_{n_{num}}^{(num)}\right)^{\dagger}\mathbf{s}_{n_{num}}^{(num)}$ perfectly removes all Intra-NI, which is a part of MUI. The suppression of Intra-NI with ZF precoders can be expressed as given in equations (8) and (9) for, respectively, user 1 and user 2.

$$\sum_{m_t=1}^{M_t}\mathbf{hf}_{2,m_t}^{(1)}[n_1]\mathbf{v}_{m_t}^{(1)}[n_1] = 0, \quad n_1 = 1, \ldots, N_1, \tag{8}$$

$$\sum_{m_t=1}^{M_t}\mathbf{hf}_{1,m_t}^{(2)}[n_2]\mathbf{v}_{m_t}^{(2,n)}[n_2] = 0, \quad n = 1, \ldots, N \,\&\, n_2 = 1, \ldots, N_2. \tag{9}$$

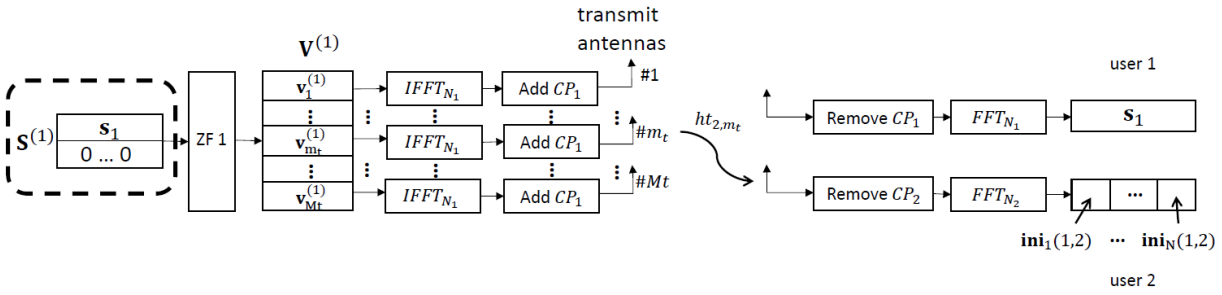

(a) Transmission where zero-signal is prepared for user 2. At the receiver side, user 2 will only receives INI

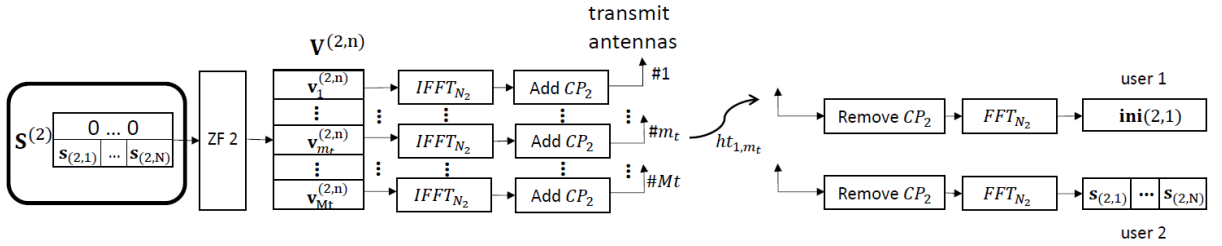

(b) Transmission where zero-signal is prepared for user 1. At the receiver side, user 1 will only receives INI

FIGURE 5. Systems used when analysing different INIs.

It is worthwhile to note that equation (8) and (9) are satisfied only when $M_t \gg M_r$, permitting that the ZF precoders perform well and are able to suppress completely Intra-numerology MUI. Obviously, this is not applicable in SISO systems and even more, in classical MIMO, where the number of the BS transmitting antennas is not sufficiently high. Thus, the study that we will conduct in the next section, to analyse the INI occurred between users using different numerologies, will be valid only for massive MIMO-OFDM systems. Also, it will be different to the ones conducted previously for SISO and classical MIMO systems. Concerning the INI between users using different numerologies, the received signal can be written as

$$\mathbf{y}_1[n_1] = \mathbf{s}_1[n_1] + \mathbf{ini}^{(2,1)}[n_1] + \mathbf{b}_1[n_1], \quad n_1 = 1, \ldots, N_1, \tag{10}$$

$$\mathbf{y}_{2,n}[n_2] = \mathbf{s}_{2,n}[n_2] + \mathbf{ini}_n^{(1,2)}[n_2] + \mathbf{b}_{2,n}[n_2], \quad n_2 = 1, \ldots, N_2. \tag{11}$$

where $\mathbf{y}_1$ is the received signal of user 1, $\mathbf{y}_{2,n}$ is the n-th received signal of user 2, $\mathbf{ini}^{(2,1)}$ and $\mathbf{ini}_n^{(1,2)}$ are INI from numerology 2 to numerology 1 and INI from numerology 1 to n-th numerology 2 symbol, respectively. $\mathbf{b}_1$ and $\mathbf{b}_{2,n}$ are receiver noise whose entries are i.i.d circularly-symmetric complex Gaussian distribution with zero-mean and $\sigma_b{}^2$ variance.

The next section will give the theoretical expressions of these two INI and analyse the impact of SCS, channel selectivity and power allocation. To do that, we consider noise-less channel in order to only study the received INI.

III. INTER-NUMEROLOGY INTERFERENCE ANALYSIS

A. INI FROM NUMEROLOGY 1 WITH N_1 TO NUMEROLOGY 2 WITH $N_2 = N_1/N$

First, we consider the user 2 using numerology 2, which is with smaller IFFT/FFT size N_2.

Corollary 1: Using the proposed transceiver design for a massive MIMO-OFDM based mixed numerologies SS transmission, the user using the small numerology (i.e. smaller IFFT/FFT size) is always protected by the ZF. Thus, we have:

$$\mathbf{ini}_n^{(1,2)} = 0 \qquad n = 1, \ldots, N. \tag{12}$$

Proof: If we activate only the dash-line block in Fig. 1, all-zero signal is transmitted for user 2. As the ZF precoder eliminates all MUI, at user 2, we receive only INI caused by numerology 1. The transmission chain is shown on Fig. 5 (a). One symbol modulated with numerology 1 corresponds to N INI symbols for user 2. INI comes from the unequal size of IFFT/FFT, which is indicated in Fig. 6 (a) where the FFT window of numerology 2 is smaller than that of numerology 1. If we consider the transmission between transmit antenna mt and user 2, the n-th received symbol, in frequency domain, can be expressed as:

$$\mathbf{y}_{2,n,m_t} = \mathbf{G}^{(1)}\mathbf{W}_n^{(1)} Diag\left(\mathbf{hf}_{2,m_t}^{(1)}\right)\left(\mathbf{v}_{m_t}^{(1)}\right)^T. \tag{13}$$

where $\mathbf{y}_{2,n,m_t} \in \mathbb{C}^{1\times N_2}$ is the received n-th symbol on user 2 with numerology 2, transmitting from the mt-th transmit antenna. $\mathbf{G}^{(1)} = \mathbf{DFT}_{N_2} \in \mathbb{C}^{N_2\times N_2}$, $\mathbf{hf}_{2,m_t}^{(1)} \in \mathbb{C}^{1\times N_1}$ is the MIMO channel frequency response between mt-th transmitting antenna and user 2. $\mathbf{W}_n^{(1)} \in \mathbb{C}^{N_2\times N_1}$ is the n-th $N_2 \times N_1$

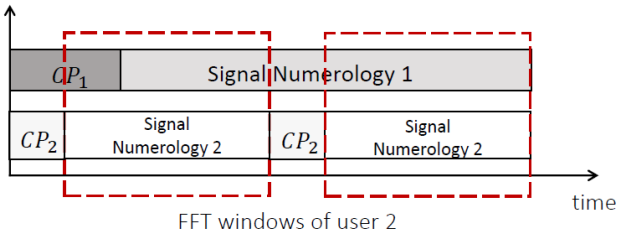

(a) INI from user 1 to user 2

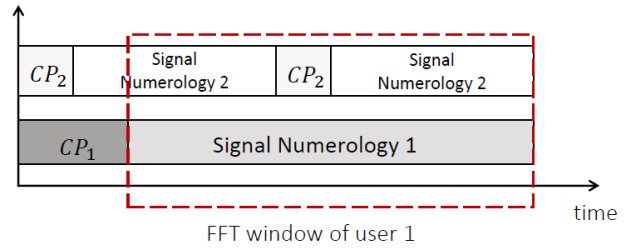

(b) INI from user 2 to user 1

FIGURE 6. FFT windows and INI on the receiver side.

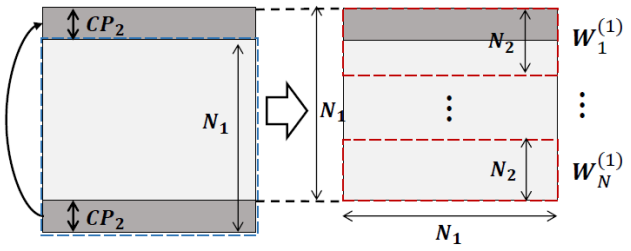

FIGURE 7. Structure of matrix $\mathbf{W}^{(1)}$ and matrices $\mathbf{W}_n^{(1)}$. The blue dash block is $\mathbf{IDFT}_{N_1}$, we rotate the last $CP_2 \times N_1$ part above to get $\mathbf{W}^{(1)}$ as shown on the left side. Then, $\mathbf{W}_n^{(1)}$ is the n-th $N_2 \times N_1$ part of $\mathbf{W}^{(1)}$ as the red dash blocks shown on the right side.

part of matrix $\mathbf{W}^{(1)}$, where $\mathbf{W}^{(1)} \in \mathbb{C}^{N_1 \times N_1}$ is a rotated version of matrix IDFT. The structure of matrix $\mathbf{W}^{(1)}$ is shown on Fig. 7.

The INI from numerology 1 to numerology 2 can then be seen as the summation of $\mathbf{y}_{2,n,m_t}$ in (13) over all transmitting antennas. It is given by equation (14):

$$\begin{aligned}\mathbf{ini}_n^{(1,2)} &= \sum_{mt=1}^{M_t} \mathbf{y}_{2,n,m_t} \\ &= \sum_{m_t=1}^{M_t} \mathbf{G}^{(1)}\mathbf{W}_n^{(1)} Diag\left(\mathbf{hf}_{2,m_t}^{(1)}\right)\left(\mathbf{v}_{m_t}^{(1)}\right)^T \\ &= \mathbf{G}^{(1)}\mathbf{W}_n^{(1)} \sum_{n_1=1}^{N_1}\sum_{m_t=1}^{M_t} \mathbf{hf}_{2,m_t}^{(1)}[n_1]\mathbf{v}_{m_t}^{(1)}[n_1]. \quad (14)\end{aligned}$$

According to (8), one can easily note that $\sum_{m_t=1}^{M_t} \mathbf{hf}_{2,m_t}^{(1)}[n_1]\mathbf{v}_{m_t}^{(1)}[n_1] = 0$, giving that,

$$\mathbf{ini}_n^{(1,2)} = 0 \quad n = 1, \ldots, N. \quad (15)$$

Here, we demonstrate theoretically that there is no INI from numerology 1 to numerology 2 as our proposed precoding scheme protects all the subcarriers received by user 2.

Remark 1: Performance of users using small numerology (IFFT/FFT size) are perfect in any configuration of SCS, channel selectivity and power allocation.

Thus, unlike the SISO/classical MIMO, where INI is occurred on small numerology (IFFT/FFT size) [20], [23], using the proposed transceiver design for massive MIMO-OFDM, the INI of users with small IFFT/FFT size is completely suppressed. This will enable the advancement of massive MIMO technology deployment in the next generation of cellular networks.

In contrast to user 2, transmission of user 1 is not perfectly protected by the ZF precoder, the INI analysis will be given in the next part of this section.

B. INI FROM NUMEROLOGY 2 WITH N_2 TO NUMEROLOGY 1 WITH $N_1 = N \times N_2$

In this section, we consider the received INI signal on user 1.

Corollary 2: By using the proposed precoding scheme in massive MIMO-OFDM mixed numerologies SS transmission, users using large numerology (i.e. larger IFFT/FFT size) are not totally protected by the ZF precoders

Proof : If we activate only the solid-line block on Fig. 1, zeros are transmitted for user 1. Fig. 5 (b) illustrates the transmission in this case where zeros are prepared for user 1 and the received signal on user 1 is the INI caused by signal of user 2. As $N_1 = N \times N_2$, N symbols with numerology 2 correspond to one symbol with user 1. Fig. 6 (b) illustrates the unequal FFT window on the receiver side which causes the INI. The total INI is the summation of INI from each symbol modulated with numerology 2 and can be expressed as:

$$\mathbf{ini}^{(2,1)} = \sum_{n=1}^{N} \mathbf{ini}_n^{(2,1)} = \sum_{n=1}^{N}\sum_{n_2=1}^{N_2} \mathbf{ini}_{n,n_2}^{(2,1)}. \quad (16)$$

where $n = 1, .., N$, $n_2 = 1, \ldots, N_2$, $\mathbf{ini}_n^{(2,1)}$ is the influence from the n-th symbol with numerology2 and $\mathbf{ini}_{n,n_2}^{(2,1)}$ is the influence from the n_2-th subcarrier in n-th symbol with numerology2. Similar as the previous section, if we concentrate on the mt-th transmit antenna, the theoretical expression of the received signal on user 1 can be derived as:

$$\mathbf{y}_{1,n,m_t} = \begin{cases} \mathbf{G}_1^{(2)}\mathbf{W}_1^{(2)} Diag\left(\mathbf{hf}_{1,m_t}^{(1)}\right)\mathbf{G}_2^{(2)}\mathbf{W}_2^{(2)}\left(\mathbf{v}_{m_t}^{(2,n)}\right)^T \\ for \quad n = 1, \\ \mathbf{G}_2^{(2)}\mathbf{ID}_n^{(2)}\mathbf{W}_3^{(2)} Diag\left(\mathbf{hf}_{1,m_t}^{(1)}\right)\mathbf{G}_2^{(2)}\mathbf{W}_2^{(2)}\left(\mathbf{v}_{m_t}^{(2,n)}\right)^T \\ for \quad n = 2, \ldots, N. \end{cases} \quad (17)$$

where $\mathbf{y}_{1,n,m_t}$ is the received INI caused by the n-th symbol with numerology 2. $\mathbf{hf}_{1,m_t}^{(1)} \in \mathbb{C}^{1 \times N_1}$ is the MIMO channel frequency response between the mt-th transmitting antenna

and user 1. All the other matrices in the expression are:

$$\begin{aligned}
\mathbf{G}_1^{(2)} &= \left[\mathbf{0}_{N_1\times CP_1}\ \mathbf{DFT}_{N_1}\right] \in \mathbb{C}^{N_1\times(N_1+CP_1)},\\
\mathbf{G}_2^{(2)} &= \mathbf{DFT}_{N_1} \in \mathbb{C}^{N_1\times N_1},\\
\mathbf{W}_1^{(2)} &= \begin{bmatrix}\mathbf{IDFT}_{N_1}\\ \mathbf{0}_{CP_1\times N_1}\end{bmatrix} \in \mathbb{C}^{(N_1+CP_1)\times N_1},\\
\mathbf{W}_3^{(2)} &= \mathbf{IDFT}_{N_1} \in \mathbb{C}^{N_1\times N_1},\\
\mathbf{ID}_n^{(2)} &= \begin{bmatrix}\mathbf{0}_{T_1\times(N_1/2)} & \mathbf{0}_{T_1\times(N_1/2)}\\ \mathbf{I}_{T_2} & \mathbf{0}_{T_2\times(N_1-T_2)}\\ \mathbf{0}_{T_3\times(N_1/2)} & \mathbf{0}_{T_3\times(N_1/2)}\end{bmatrix} \in \mathbb{C}^{N_1\times N_1}.
\end{aligned}$$

for matrix $\mathbf{ID}_n^{(2)}$, we have

$$\begin{cases}
T_1 = N_1 - (N-n+1)(N_2+CP_2),\\
T_2 = \begin{cases} N_2+CP_2+D & for \quad n=2,\ldots,N-1\\ N_2+CP_2 & for \quad n=N,\end{cases}\\
T_3 = \begin{cases} (N-n)(N_2+CP_2)-D & for \quad n=2,\ldots,N-1\\ (N-n)(N_2+CP_2) & for \quad n=N.\end{cases}
\end{cases} \tag{18}$$

The structure of matrix $\mathbf{W}_2^{(2)} \in \mathbb{C}^{N_1\times N_2}$ is shown on Fig.8.

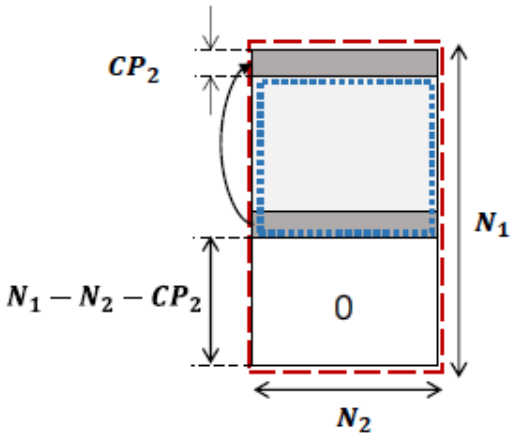

FIGURE 8. Structure of matrix $\mathbf{W}_2^{(2)}$ with red dash box. The blue dot block is $\mathbf{IDFT}_{N_2}$, we copy the last $CP_2 \times N_2$ part above and add zeros below to extend the dimension to $N_1 \times N_2$.

The signal received on user 1 is the summation from all transmit antennas, thus:

$$\mathbf{ini}_n^{(2,1)} = \sum_{m_t=1}^{M_t} \mathbf{y}_{1,n,m_t}. \tag{19}$$

From (17), we can rewrite (19):

$$\mathbf{ini}_n^{(2,1)} = \sum_{m_t=1}^{M_t} \mathbf{E}_n Diag\left(\mathbf{hf}_{1,m_t}^{(1)}\right) \mathbf{Z}\left(\mathbf{v}_{m_t}^{(2,n)}\right)^T. \tag{20}$$

where

$$\mathbf{E}_n \in \mathbb{C}^{N_1\times N_1} = \begin{cases} \mathbf{G}_1^{(2)}\mathbf{W}_1^{(2)} & for \quad n=1,\\ \mathbf{G}_2^{(2)}\mathbf{ID}_n^{(2)}\mathbf{W}_3^{(2)} & for \quad n=2,\ldots,N.\end{cases} \tag{21}$$

$\mathbf{Z} = \mathbf{G}_2^{(2)}\mathbf{W}_2^{(2)} \in \mathbb{C}^{N_1\times N_2}$ is identical for all symbols. Then, the INI on n_1-th subcarrier with numerology 1 from n-th symbol with numerology 2 can be expressed as:

$$\begin{aligned}
&\mathbf{ini}_n^{(2,1)}[n_1]\\
&= \sum_{n_1'=1}^{N_1}\sum_{n_2=1}^{N_2}\sum_{m_t=1}^{M_t} \mathbf{E}_n(n_1,n_1')\mathbf{hf}_{1,m_t}^{(1)}[n_1']\mathbf{Z}(n_1',n_2)\mathbf{v}_{m_t}^{(2,n)}[n_2]\\
&= \sum_{n_1'=1}^{N_1}\sum_{n_2=1}^{N_2} \mathbf{E}_n(n_1,n_1')\mathbf{Z}(n_1',n_2)\sum_{m_t=1}^{M_t}\mathbf{hf}_{1,m_t}^{(1)}[n_1']\mathbf{v}_{m_t}^{(2,n)}[n_2].
\end{aligned} \tag{22}$$

where $n_1 = 1,\ldots,N_1, n_1' = 1,\ldots,N_1, n_2 = 1,\ldots,N_2$ and $m_t = 1,\ldots,M_t$.

According to the expression of $\mathbf{ini}_n^{(2,1)}$ in (22), (9) is not satisfied due to the different frequency response of a selective channel, $\mathbf{hf}_{1,m_t}^{(1)}[n_1] \neq \mathbf{hf}_{1,m_t}^{(2)}[n_2]$, where $n_1 = 1,\ldots,N_1, n_2 = 1,\ldots,N_2$. We can conclude that in a selective channel, user 1 will suffer from INI caused by user 2.

Remark 2: In a constant channel, $\mathbf{ini}^{(2,1)}$ *is zero due to the channel frequency response characteristic.*

The two MIMO channels $\mathbf{hf}_{1,m_t}^{(1)} = FFT(\mathbf{ht}_{1,m_t}, N_1) \in \mathbb{C}^{1\times N_1}$ and $\mathbf{hf}_{1,m_t}^{(2)} = FFT(\mathbf{ht}_{1,m_t}, N_2) \in \mathbb{C}^{1\times N_2}$ are two frequency responses of the same impulse response with different length. When the channel is constant, we have:

$$\mathbf{hf}_{1,m_t}^{(1)}[n_1] = \mathbf{hf}_{1,m_t}^{(2)}[n_2]. \tag{23}$$

where $n_1 = 1,\ldots N_1, n_2 = 1,\ldots N_2$.

From (9) and (23), all the elements inside the two frequency response are equal. Then, for all subcarriers of user 1, we have:

$$\begin{aligned}
&\mathbf{ini}_n^{(2,1)}[n_1]\\
&= \sum_{n_1'=1}^{N_1}\sum_{n_2=1}^{N_2} \mathbf{E}_n(n_1,n_1')\mathbf{Z}(n_1',n_2)\sum_{m_t=1}^{M_t}\mathbf{hf}_{1,m_t}^{(2)}[n_2]\mathbf{v}_{m_t}^{(2,n)}[n_2]\\
&= 0.
\end{aligned} \tag{24}$$

Unlike the SISO and classical MIMO systems, massive MIMO is able to support mixed numerologies and no INI is generated when the channel is flat-fading. This finding is valid only for massive MIMO when the proposed transceiver design is employed.

Remark 3: Channel selectivity and difference between N_1 *and* N_2 *increase the* $\mathbf{ini}^{(2,1)}$.

When the channel is frequency-selective, vector $\mathbf{hf}_{1,m_t}^{(1)}$ is the interpolation of vector $\mathbf{hf}_{1,m_t}^{(2)}$. In a frequency-selective channel, $N-1$ values are added between every two points in $\mathbf{hf}_{1,mt}^{(2)}$ to construct vector $\mathbf{hf}_{1,m_t}^{(1)}$. From this characteristic, we have:

$$\mathbf{hf}_{1,m_t}^{(1)}[(n_2-1)N+1] = \mathbf{hf}_{1,m_t}^{(2)}[n_2]. \tag{25}$$

where $n_2 = 1,\ldots N_2$.

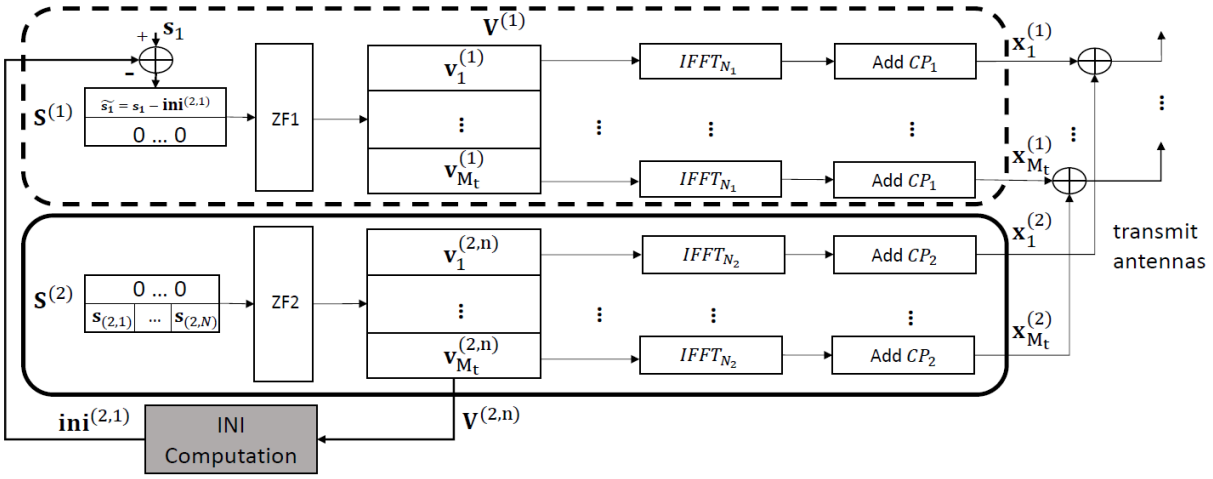

FIGURE 9. INI cancellation scheme at the BS, where there is INI computation after ZF of user 2 and the pre-calculated INI is suppressed for user 1.

For the interference, we can first consider the n_2-th subcarrier of the n-th symbol with numerology 2. Its impact on the n_1-th subcarrier with numerology 1 is derived in (22). From (25) and (9), the influence of n_2-th subcarrier is zero only when $n_1' = (n_2 - 1)N + 1$, because in this case, we have $\mathbf{hf}_{1,m_r}^{(1)}[n_1] = \mathbf{hf}_{1,m_r}^{(2)}[n_2]$. For other values of n_1 ($n_1 \neq (n_2 - 1)N + 1$), the difference between $\mathbf{hf}_{1,m_r}^{(1)}[n_1]$ and $\mathbf{hf}_{1,m_r}^{(2)}[n_2]$ has a close relationship with the channel selectivity and the difference between N_1 and N_2. Greater selectivity and greater difference between N_1 and N_2 cause greater difference on the two channel frequency responses, which leads to greater interference.

Remark 4: Power allocation for different users has a direct influence on interference $\mathbf{ini}^{(2,1)}$.

For the sake of simplicity and to focus on the INI analysis, in this paper, we adopt a simple power allocation scheme, where the power assigned to the m_r-th user (p_{m_r}) is proportional to the inverse of its path-loss $\sqrt{\alpha_{m_r}}$. The power allocation for each user is:

$$\mathbf{P} = \frac{\rho}{M_t}\mathbf{A}^{-1}. \tag{26}$$

where ρ is a normalization factor which ensures that the power constraint $tr(\mathbf{P}) = p_{Tx}$ is met. $\mathbf{P} = Diag(p_1, \ldots, p_{M_r})$ and $\mathbf{A} = Diag(\alpha_1, \ldots, \alpha_{m_r})$. Then, greater large-scale fading in user m_r leads to greater transmitting power for that user.

In our system, having two users with different path-loss, the signals' power after precoding satisfy:

$$\frac{p_1}{p_2} = \frac{tr(\mathbf{V}^{(1)})}{tr(\mathbf{V}^{(2)})} = \frac{\alpha_2}{\alpha_1}. \tag{27}$$

For example, if $\alpha_2 < \alpha_1$, which indicates that user 2 is farther away from the BS than user 1. After the precoding, we will have $p_2 > p_1$ $\left(tr(\mathbf{V}^{(1)}) > tr(\mathbf{V}^{(2)})\right)$. From (17), the received INI power on user 1 is proportional to the power of $\mathbf{V}^{(2)}$. That is to say, if user 2 is farther away from the BS, i.e. $\alpha_2 < \alpha_1$, user 1 receive more INI because of the increased transmitting power for user 2.

In summary, from the analysis in this section, one can observe that, first, INI from numerology 2 with N_2 to numerology 1 with $N \times N_2$ occurs in our proposed system. Then, in a frequency-selective channel, the INI increases due to the difference in IFFT/FFT size, channel selectivity and power allocation. We recall that the derived analytical INI models (equation (14) and (20)) is valid only for massive MIMO (i.e. $M_t \gg M_r$), where the hypothesis in equation (8) and (9) hold.

IV. INI CANCELLATION

As analysed in the previous sections, only numerology with large IFFT/FFT size suffers from INI from numerologies with small IFFT/FFT size. In this section, we introduce an INI cancellation scheme with the aid of the analytical results of INI presented in the previous sections. One of the main idea in massive MIMO downlink transmission is to reduce the complexity of the receiver while maintaining the good transmission quality by doing all process at the BS [11]. Also, in massive MIMO, the full channel state is only estimated in the uplink transmission. For the downlink transmission, the uplink channel estimation is used for the precoding, but differences between the uplink and downlink channels are adjusted by a reciprocity calibration process [28]. In this regard, the proposed INI cancellation method implements at the BS side, which does not add any complexity to the receivers.

Fig. 9 shows the scheme of the proposed INI cancellation method at the BS side. The main idea is to calculate the INI from numerology 2 to numerology 1 in advance with the knowledge of the MIMO channel response and signals after precoding of user 2. Then, in the transmission part, instead of transmitting $\mathbf{s}_1$, we transmit $\widetilde{\mathbf{s}}_1 = \mathbf{s}_1 - \mathbf{ini}^{(2,1)}$. This change does not bring any INI at user 2, as we have demonstrated in

TABLE 1. Complexity comparison.

Module		Analytical expression	Complexity under the configuration	
Transmitter	ZF precoders	$(2M_tM_r^2 + {M_r}^3)N_1 + (2M_tM_r^2 + {M_r}^3)N_2$	1241088	3596288
	ZF precodings	$M_tM_rN_1 + 2M_tM_rN_2$	409600	
	IFFTs	$M_tN_1log_2(N_1) + 2M_tN_2log_2(N_2)$	1945600	
INI cancellation		$2M_tN_1L$	1843200	

section III.A, that our proposed transmission scheme protects perfectly the transmission of user 2. In INI cancellation, the transmit power $p_{Tx} = p_u + p_{ini}$, where p_u is the power allocated for users and p_{ini} is the power for INI cancellation. It is worth noting that ρ, in equation (26), is ajusted in order to satisfy the constraint specified by the total transmit power p_{Tx} while taking in account the p_{ini}. According to the several conducted simulations, the p_{ini} is negligible compared to the power allocated to users (p_u) and it is worthwhile to mention that this will lead to a negligible signal-to-noise (SNR) loss.

From analysis in section III.B, for each subcarrier of user 1, the interference comes from all subcarriers of user 2, as we can observe in the theoretical expression in equation (22), a summation over N_2 subcarriers. In fact, for subcarrier n_1 of user 1, although there is difference according to its parity, the most part of the interference always corresponds to subcarrier $n_2 = \left\lceil \frac{n_1}{2} \right\rceil$ and its neighbours. Fig. 10 (a) and (b) show the normalized interference power occurred, respectively, on subcarrier $n_1 = 500$ and $n_1 = 501$, versus the user 2's subcarrier index n_2. Here, we consider $N_1 = 1024$ and $N_2 = 512$. It is clear that the main interference comes approximately from the neighbours around subcarrier $n_2 = \left\lceil \frac{n_1}{2} \right\rceil$. Summation in (22) can thus be limited to few subcarriers around $n_2 = \left\lceil \frac{n_1}{2} \right\rceil$.

In the cancellation process, the estimated $\mathbf{ini}^{(2,1)}$ of equation (22) can be computed over only several subcarriers on numerology 2, as shown on these figures, two windows of length L. This will reduce the complexity of the proposed transceiver with INI cancellation.

With the configuration $N_1 = 1024, N_2 = 512, M_t = 100$ and $M_r = 2$, it is possible to assess the complexity of the proposed INI cancellation method and it is given in TABLE 1. For IFFT/FFT computational complexity, we have used the complexity of the Radix-2 case [29]. For matrix inversion (in computation of ZF precoding matrix), we have used the computational complexity of Gauss-Jordan elimination technique [30]. Here, we consider the number of complex multiplications for each symbol of user 1 and an INI calculation window length $L = 9$. The complexity of the original transmitter includes the complexity of the computation of two ZF precoders, the two ZF precoding processing and the IFFT stages, which are given in detail, for each part, in TABLE 1.

According to the results illustrated in TABLE 1, complexity is influenced by the number of transmitting antennas at the BS and the largest IFFT/FFT size. It is worth mentioning that

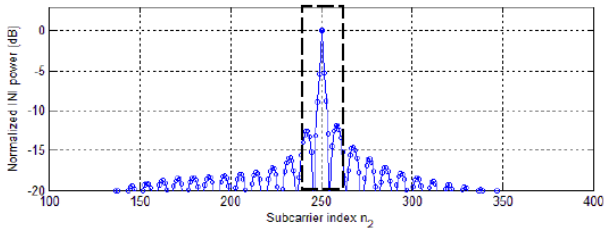

(a) Interference on subcarrier $n_1 = 500$, where most inteference come from subcarrier $n_2 = 250$ and its neighbours.

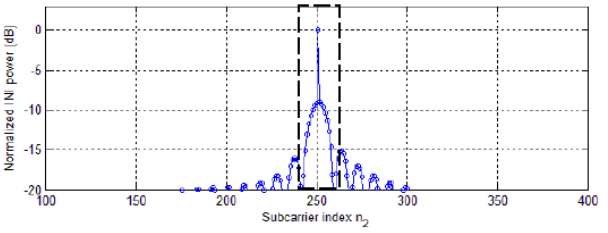

(b) Interference on subcarrier $n_1 = 501$, where most inteference come from subcarrier $n_2 = 251$ and its neighbours.

FIGURE 10. Interference on certain subcarriers of user 1. $N_1 = 1024$, $N_2 = 512$.

the chosen window length (Fig.10) does not impact on the complexity of our INI cancellation method. This is due to the fact that the most impacted adjacent subcarriers remain the same whether the channel selectivity changes or not. In our configuration, the INI cancellation complexity represents 51.25% of the original transceiver design. Although the INI cancellation increases the total complexity of the system, but simulation results prove the high capability in eliminating the INI, which will be shown in the next section.

What is more is that, the proposed INI cancellation scheme can be adapted to any system using more than two numerologies. The computation of INI always starts from numerology with the smallest IFFT/FFT size. Numerology with the largest IFFT/FFT size can be corrected by suppressing INIs from all the other numerologies.

V. SIMULATION RESULTS

In this section, we evaluate the accuracy of the derived analytical expressions for INI in a mixed numerologies SS massive MIMO-OFDM downlink system. The BS is equipped with $M_t = 100$ antennas and two single-antenna users ($M_r = 2$) that are using two different numerologies but sharing the same band. Two pairs of numerologies and

four different channel models are considered. A 16-QAM with Gray mapping is considered. We define the first pair of numerologies with $N_1 = 1024, N_2 = 512, CP_1 = 72, CP_2 = 36$ and the second pair with $N_1 = 1024, N_2 = 256, CP_1 = 72, CP_2 = 18$. The time-domain channel responses $\mathbf{ht}_{mr,mt}[d] = c_d$ have i.i.d. circularly symmetric Gaussian distributed values with zero mean and unit variance where $d = 1, \ldots, D$. The four wireless channels are modelled as a tap delay line with $D = 1, 2, 8, 18$ taps respectively. It has to be noted that in all cases, the CP length are sufficient to suppress the ISI induced by the channel.

To evaluate the INI, we first consider the transmission without noise. We define the normalized mean-square error (NMSE) as:

$$\text{NMSE}_{num} = \frac{\| \mathbf{y}_{num} - \mathbf{s}_{num} \|^2}{\| \mathbf{s}_{num} \|^2}, \quad num = 1, 2. \tag{28}$$

We recall that $\mathbf{y}_{num}$ is the received symbols and $\mathbf{s}_{num}$ is the transmitted symbols.

TABLE 2. NMSE (dB) of user of interest with interfering numerology and different channels.

User of Interest	user1 ($N_1 = 1024$)		user2 ($N_2 = 512$)	user2 ($N_2 = 256$)
Interfering User	user2($N_2 = 512$)	user2($N_2 = 256$)	user1($N_1 = 1024$)	
$D = 1$	-300	-300	-300	-300
$D = 2$	-52	-48	-300	-300
$D = 8$	-42	-37	-300	-300
$D = 18$	-38	-33	-300	-300

The NMSE values in dB under different conditions for the user of interest with the transmission system introduced in this paper are shown on TABLE 2. Note that all simulation results shown in TABLE 2 are with $P_1 = P_2$. One can note on TABLE 2, that, transmissions for user 2 which uses small IFFT/FFT size is always with the best quality (NMSE value of around -300 dB), no matter what IFFT/FFT size or channel selectivity. It has to be noted that the value -300 dB is related to the fact that: (a) We have used floating point operation on Matlab. (b) We have a very small number of users (2 users in the simulations). When the number of users increases, the degrees of freedom will decrease and the NMSE values will be affected. Fixed point operation together with imperfect channel estimation will also degrade this NMSE. These results match perfectly with the analysis done in section III.A showing that numerology 2 with small IFFT/FFT size does not suffer from the INI from numerology 1. However, in a frequency-selective channel, when the difference between IFFT/FFT size increases, user 1 suffers more INI from numerology 2. For example, for the same frequency-selective channel with $D = 2$, the performance of user 1 is worse when interference is from $N_2 = 256$ than that from $N_2 = 512$ (4 dB difference). This difference may lead to worse transmitting quality. Meanwhile, when we compare the performance of the same pair of N_1 and N_2 under different channel selectivities, we can observe that the more selective the channel is, the worse is the user1's performance. For $N_1 = 1024, N_2 = 512$, there is 10 dB of degradation under channel $D = 8$ compared to channel $D = 2$ and 14 dB under channel $D = 18$. For $N_1 = 1024, N_2 = 256$, the degradation goes to 11 dB and 15 dB. These results confirm our analysis in section III.B.

TABLE 3. Scenario parameters and simulation results on user 1.

(a) Different scenarios

	distance user 2/BS (km)	path-loss of user 2 (dB)	distance user 1/BS (m)	path-loss of user 1 (dB)	α_1/α_2 (dB)
case 1	1	128.1	300	108.44	20
case 2	1	128.1	250	105.46	23
case 3	1	128.1	200	101.82	26

(b) NMSE values before and after INI cancellation

User of Interest	user1 ($N_1 = 1024$)			
Interfering User	user2($N_2 = 512$)		user2($N_2 = 256$)	
α_1/α_2 (dB)	original (dB)	corrected (dB)	original (dB)	corrected (dB)
20	-22	-300	-18	-300
23	-19	-300	-14	-300
26	-16	-300	-11	-300

If we look at TABLE 2, the NMSE of INI is always very small (-33 dB for the maximum value) and should have a limited impact for classical SNRs. Nevertheless, it has to be pointed out that these values are for users with same path-loss: $\alpha_1 = \alpha_2$ ($\alpha_1/\alpha_2 = 0$ dB). If we consider a more realistic scenario with the long time evolution (LTE) path-loss model given by equation (29) [31]

$$\text{Pathloss(dB)} = 128.1 + 37.6\log_{10}(d_k) \tag{29}$$

where d_k is the distance from the BS in km. Then, values of α_1 and α_2 will change.

From the analysis in previous sections and the simulation results shown in TABLE 2, user 2 is performed with the best quality, hence, in the following simulations, we focus on the transmission of user 1. For example, in a scenario with a cell radius equals to 1 km, we have the following path-loss attenuations given in TABLE 3 sub-table (a), for different user/BS distances.

TABLE 3 sub-table (b) shows the relationship between path-loss and system performance, where the number of channel taps D is fixed at $D = 8$.

It can be seen that, user 1 suffers greater INI with the growth of path-loss on user 2. Compared with TABLE 2, when $N_1 = 1024$, $N_2 = 512$ and $D = 8$, there is degradation of 20 dB when $\alpha_1/\alpha_2 = 20$ dB compared to $\alpha_1/\alpha_2 = 0$ dB. This degradation increase to 23 dB and 26 dB when $\alpha_1/\alpha_2 =$ 23 dB and $\alpha_1/\alpha_2 = 26$ dB. These results perfectly match our analysis in section III.B. It can be also found in the lower sub-table that, after the INI cancellation implemented at the BS, transmission of user 1 performs as well as user 2, reaching -300 dB for all values of path-loss.

To confirm the analysis of INI on user 1, Fig.11 presents the bit error rate (BER) vs. E_b/N_0 using $N_1 = 1024$, $N_2 = 512$ and $D = 18$.

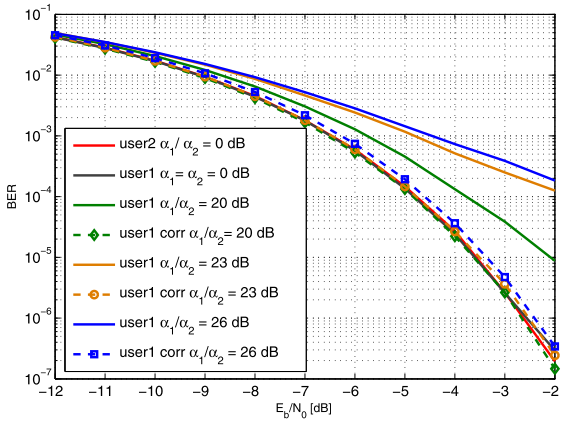

FIGURE 11. BER performance with and without INI cancellation on user 1. $\alpha_1/\alpha_2 = 0, 20, 23$ and 26 dB.

From Fig.11, we can observe that the performance of user 1 is significantly declined when the path-loss of user 2 increases. For example, we can compare $\alpha_1/\alpha_2 = 0$ dB and $\alpha_1/\alpha_2 = 26$ dB. When $E_b/N_0 = -3$ dB, user 1 can archive $BER \leq 10^{-6}$ when $\alpha_1/\alpha_2 = 0$ dB while the SER of user 1 is larger than 10^{-4} when $\alpha_1/\alpha_2 = 26$ dB.

Also, in Fig. 11, the BER vs. E_b/N_0 performance with INI cancellation is presented for user 1 and user 2 with different path-loss on user 2. $N_1 = 1024$, $N_2 = 512$. All the dash lines represent the BER after the implementation of the cancellation algorithm introduced in section IV. It can be observed that the algorithm improves the performance of user 1 under different path-loss cases. After the cancellation, user 1 and user 2 have a negligible BER loss, even when $\alpha_1/\alpha_2 = 26$ dB. We can also observe a slight BER mismatch when the path-loss of user 2 becomes great (the dash-blue curve), which is mainly caused by the introduced INI cancellation power p_{ini}. However, as we explained in section IV, this effect is negligible. Until now, we assume that in all simulations, the BS knows perfectly the channel state information (CSI). However, it is worth noticing that the proposed INI cancellation method is as sensitive to the imperfect CSI as the ZF precoder.

The simulations above give the results of a simple cell where only two different numerologies are taken into consideration and each group using the same numerology has only one user. In practice, each group can have several users and there can be several groups in one cell. Fig. 12 gives a diagram of a cell with $M_t = 100$, $M_r = 30$, where users are uniformly distributed in the ring around the BS, with inner radius $r_1 = 200$ m and outer radius $r_2 = 1000$ m. The thirty users are divided into three groups, where Group 1 contains user No. 1 to No. 10, Group 2 contains user No. 11 to No. 20 and Group 3 contains user No. 21 to No. 30, using three different numerologies with IFFT/FFT size of 1024, 512 and 256 respectively.

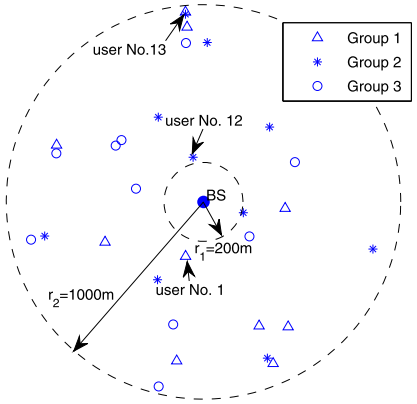

FIGURE 12. User distribution in a ring where BS is in the center. The inner radius $r_1 = 200$ m and the outer radius $r_2 = 1000$ m. $M_t = 100$, $M_r = 30$.

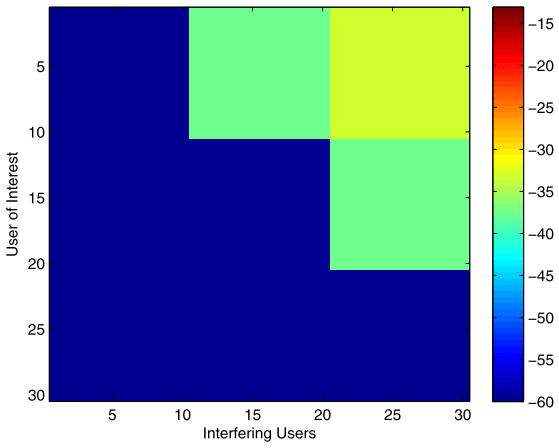

FIGURE 13. NMSE values for different users without considering the path-loss. Group 1: user No.1 to No.10 with $N_1 = 1024$. Group 2: user No.11 to No.20 with $N_2 = 512$. Group 3: user No.21 to No.30 with $N_3 = 256$. Channel taps $D = 18$.

Fig. 13 represents the INI between different users in the cell using our proposed transceiver design regardless of path-loss under a frequency-selective channel with $D = 18$, where the x axis indicates the interfering user index, the y axis indicates the user of interest (UoI) and the color indicates the NMSE values of the UoI. We can observe that in most cases (the dark-blue part), there is no INI between users. Especially, for the users from group 3 (UoI No. 21 to No. 30) using

IFFT/FFT size equals to 256, the other two groups do not generate any INI on them. Beside, for the cases where INI is generated, the NMSE values are around −35 dB (also shown on TABLE 2, which is to say, there is no need of implementing INI cancellation even they belong to different numerologies if users have similar path-loss.

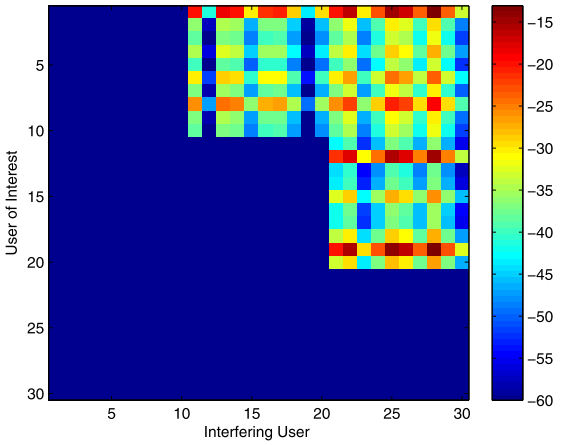

FIGURE 14. NMSE values for different users considering the path-loss presented on Fig.12. Group 1: user No.1 to No.10 with $N_1 = 1024$. Group 2: user No.11 to No.20 with $N_2 = 512$. Group 3: user No.21 to No.30 with $N_3 = 256$. Channel taps $D = 18$.

However, if we take the path-loss of different users shown on Fig.12 into consideration, the INI on each user changes. Fig. 14 gives the different NMSE values on different UoI belonging to different groups. As we can see on the figure, several users are significantly impacted by other users (red and orage points). For example, we can compare the different INI impacts on UoI No. 1 from user No. 12 and No. 13, where user No. 1 belongs to group 1 ($N_1 = 1024$) while user No. 12 and No. 13 belong to group 2 ($N_2 = 512$). From Fig. 14, it is clear that the INI generated from user No. 12 to user No. 1 causes the NMSE value around -40 dB (blue point) while INI from user No. 13 to user No. 1 causes the NMSE value around -20 dB (red point). In this case, it is more necessary to cancel the INI generated from user No.13 to user No.1. The difference in path-loss between users makes the different INI impact as the positions of the three users are illustrated on Fig. 12, where user No.1 and user No.12 has similar path-loss while No.1 and user No.13 has quite large difference in path-loss. In conclusion, INI cancellation is interesting or even mandatory to implement between two users belonging to two different groups, while they have great difference in path-loss.

VI. CONCLUSION

In this paper, we first introduced a new transmitting scheme designed for MU massive MIMO-OFDM based 5G which supports different services using different numerologies while sharing the same band, contrary to mixed numerologies SISO and classical MIMO systems, where users use adjacent frequency bands. Then, we investigated the performance of this mixed numerologies in massive MIMO-OFDM downlink systems. For the occurring INI in the mixed numerologies system, we derived theoretical expressions of the INI, which were checked by simulations to guide the 5G system design and parameters selection. We demonstrated that INI is generated only in frequency selective channels and only from users with large SCS to users with small SCS. Besides, theoretical INI analysis matches the simulation results showing that INI depends on the difference in SCS, the channel selectivity and the power allocation. Last but not least, based on the developed close-form INI expressions, we proposed an INI cancellation scheme which can suppress the INI at the BS side without increasing the receiver's complexity. The results showed the ability of massive MIMO-OFDM system to support mixed numerologies transmissions while all users share the same band to meet the requirements of the future wireless communication.

REFERENCES

[1] A. J. Paulraj, D. A. Gore, R. U. Nabar, and H. Bolcskei, "An overview of MIMO communications—A key to gigabit wireless," *Proc. IEEE*, vol. 92, no. 2, pp. 198–218, Feb. 2004.

[2] J. G. Andrews, S. Buzzi, W. Choi, S. V. Hanly, A. Lozano, A. C. K. Soong, and J. C. Zhang, "What will 5G be?" *IEEE J. Sel. Areas Commun.*, vol. 32, no. 6, pp. 1065–1082, Jun. 2014.

[3] T. L. Marzetta, "Noncooperative cellular wireless with unlimited numbers of base station antennas," *IEEE Trans. Wireless Commun.*, vol. 9, no. 11, pp. 3590–3600, Nov. 2010.

[4] P. Pan, H. Wang, Z. Zhao, and W. Zhang, "How many antenna arrays are dense enough in massive MIMO systems," *IEEE Trans. Veh. Technol.*, vol. 67, no. 4, pp. 3042–3053, Apr. 2018.

[5] H. Q. Ngo, E. G. Larsson, and T. L. Marzetta, "Energy and spectral efficiency of very large multiuser MIMO systems," *IEEE Trans. Commun.*, vol. 61, no. 4, pp. 1436–1449, Apr. 2013.

[6] A. S. Y. Poon, R. W. Brodersen, and D. N. C. Tse, "Degrees of freedom in multiple-antenna channels: A signal space approach," *IEEE Trans. Inf. Theory*, vol. 51, no. 2, pp. 523–536, Feb. 2005.

[7] P. Patcharamaneepakorn, S. Wu, C.-X. Wang, e.-H. M. Aggoune, M. M. Alwakeel, "Spectral, energy, and economic efficiency of 5G multicell massive MIMO systems with generalized spatial modulation," *IEEE Trans. Veh. Technol.*, vol. 65, no. 12, pp. 9715–9731, Dec. 2016.

[8] Y. Wang and J. Lee, "A ZF-based precoding scheme with phase noise suppression for massive MIMO downlink systems," *IEEE Trans. Veh. Technol.*, vol. 67, no. 2, pp. 1158–1173, Feb. 2018.

[9] *Physical Channels and Modulation*, document ETSI TS 138 211, V12.4.0, 3GPP, 2014.

[10] *Technical Specification Group Radio Access Network; NR; Physical Layer; General Description (Release 15)*, document TS 38 201, V1.0.0, 3GPP, 2017.

[11] E. G. Larsson, O. Edfors, F. Tufvesson, and T. L. Marzetta, "Massive MIMO for next generation wireless systems," *IEEE Commun. Mag.*, vol. 52, no. 2, pp. 186–195, Feb. 2014.

[12] A. A. Zaidi, R. Baldemair, H. Tullberg, H. Bjorkegren, L. Sundstrom, J. Medbo, C. Kilinc, and I. D. Silva, "Waveform and numerology to support 5G services and requirements," *IEEE Commun. Mag.*, vol. 54, no. 11, pp. 90–98, Nov. 2016.

[13] A. Osseiran, F. Boccardi, V. Braun, K. Kusume, P. Marsch, M. Maternia, O. Queseth, M. Schellmann, H. Schotten, H. Taoka, H. Tullberg, M. A. Uusitalo, B. Timus, and M. Fallgren, "Scenarios for 5G mobile and wireless communications: The vision of the METIS project," *IEEE Commun. Mag.*, vol. 52, no. 5, pp. 26–35, May 2014.

[14] S.-Y. Lien, S.-L. Shieh, Y. Huang, B. Su, Y.-L. Hsu, and H.-Y. Wei, "5G new radio: Waveform, frame structure, multiple access, and initial access," *IEEE Commun. Mag.*, vol. 55, no. 6, pp. 64–71, Jun. 2017.

[15] A. Sahin and H. Arslan, "Multi-user aware frame structure for OFDMA based system," in *Proc. IEEE Veh. Technol. Conf. (VTC Fall)*, Sep. 2012, pp. 1–5.

[16] P. Guan, D. Wu, T. Tian, J. Zhou, X. Zhang, L. Gu, A. Benjebbour, M. Iwabuchi, and Y. Kishiyama, "5G field trials: OFDM-based waveforms and mixed numerologies," *IEEE J. Sel. Areas Commun.*, vol. 35, no. 6, pp. 1234–1243, Jun. 2017.
[17] L. Zhang, A. Ijaz, P. Xiao, A. Quddus, and R. Tafazolli,"Subband filtered multi-carrier systems for multi-service wireless communications," *IEEE Trans. Wireless Commun.*, vol. 16, no. 3, pp. 1893–1907, Mar. 2017.
[18] L. Zhang, A. Ijaz, P. Xiao, and R. Tafazolli, "Multi-service system: An enabler of flexible 5G air interface," *IEEE Commun. Mag.*, vol. 55, no. 10, pp. 152–159, Oct. 2017.
[19] A. Yazar and H. Arslan, "Reliability enhancement in multi-numerology-based 5G new radio using INI-aware scheduling," *EURASIP J. Wireless Commun. Netw.*, vol. 2019, no. 1, p. 110, May 2019, doi: 10.1186/s13638-019-1435-z.
[20] X. Zhang, L. Zhang, P. Xiao, D. Ma, J. Wei, and Y. Xin, "Mixed numerologies interference analysis and inter-numerology interference cancellation for windowed OFDM systems," *IEEE Trans. Veh. Tech.*, vol. 67, no. 8, pp. 7047–7061, Apr. 2018.
[21] A. B. Kihero, M. S. J. Solaija, A. Yazar, and H. Arslan, "Inter-numerology interference analysis for 5G and beyond," in *Proc. IEEE Globecom Workshops (GC Wkshps)*, Dec. 2018, pp. 1–6.
[22] A. Yazar, B. Pekoz, and H. Arslan, "Flexible multi-numerology systems for 5G new radio," *J. Mobile Multimedia*, vol. 14, no. 4, pp. 367–394, 2018.
[23] S. Rajagopal and M. S. Rahman, "Multi-user MIMO with flexible numerology for 5G," Oct. 2016, *arXiv:1610.03056*. [Online]. Available: https://arxiv.org/abs/1610.03056
[24] J. Choi, B. Kim, K. Lee, and D. Hong, "A transceiver design for spectrum sharing in mixed numerology environments," *IEEE Trans. Wireless Commun.*, vol. 18, no. 5, pp. 2707–2721, May 2019.
[25] Q. H. Spencer, A. L. Swindlehurst, and M. Haardt, "Zero-forcing methods for downlink spatial multiplexing in multiuser MIMO channels," *IEEE Trans. Signal Process.*, vol. 52, no. 2, pp. 461–471, Feb. 2004.
[26] Q. Qin, L. Gui, B. Gong, and S. Luo, "Sparse channel estimation for massive MIMO-OFDM systems over time-varying channels," *IEEE Access*, vol. 6, pp. 33740–33751, 2018.
[27] L. Lu, G. Y. Li, A. L. Swindlehurst, A. Ashikhmin, and R. Zhang, "An overview of massive MIMO: Benefits and challenges," *IEEE J. Sel. Topics Signal Process.*, vol. 8, no. 5, pp. 742–758, Oct. 2014.
[28] J. Vieira, F. Rusek, O. Edfors, S. Malkowsky, L. Liu, and F. Tufvesson, "Reciprocity calibration for massive MIMO: Proposal, modeling, and validation," *IEEE Trans. Wireless Commun.*, vol. 16, no. 5, pp. 3042–3056, May 2017.
[29] P. Duhamel and H. Hollmann, "Split radix'fft algorithm," *Electron. Lett.*, vol. 20, no. 1, pp. 14–16, 1984.
[30] S. C. Althoen and R. Mclaughlin, "Gauss-jordan reduction: A brief history," *The Amer. Math. monthly*, vol. 94, no. 2, pp. 130–142, 1987.
[31] *Study on Channel Model for Frequencies From 0.5 to 100 GHz (Release 14)*, document TR 138 901, V14.3.0, 3GPP, 2018.

XINYING CHENG received the B.Sc. degree in measuring control technology and instruments from Southeast University, Nanjing, China, in 2017, and the M.Sc. degree in telecommunication and network from Conservatoire National des Arts et Métiers (CNAM), France, in 2018, where she is currently pursuing the Ph.D. degree with the CEDRIC Laboratory. Her research interests are in RF impairments analysis and mitigation techniques for beyond 5G multicarrier transmissions.

RAFIK ZAYANI received the Engineering, M.Sc., and Ph.D. degrees from the École Nationale d'Ingénieurs de Tunis (ENIT), in 2003, 2004, and 2009, respectively. He was with the Laboratory of Communications Systems, ENIT, from 2003 to 2005. From 2004 to 2009, he was with the Department of Telecommunication and Networking, Institut Supérieur d'Informatique (ISI), Tunis, as a Contractual Assistant Professor. Since 2005, he has been with the Innov'COM Laboratory, Sup'Com School, Tunisia. Since 2009, he has also been an Associate Professor (tenure position) with ISI, Tunisia. Since 2010, he has also been an Associate Researcher with the CEDRIC Laboratory, Conservatoire National des Arts et Métiers, France. He is currently an Established Researcher with long experience in multicarrier communications and energy efficiency enhancement by transmitter linearization techniques (baseband DPD) and PAPR reduction; high power amplifier characterization; neural networks; identification modeling and equalization; and MIMO technologies. He was involved in enhanced multicarrier waveforms, such as FBMC-OQAM, UFMC, GFDM, BF-OFDM, and WOLA-OFDM. He has contributed to several European (EMPHATIC) and French (WONG5) projects that aim at designing flexible air-interfaces for future wireless communications (5G and Beyond). He has recently been awarded the H2020 Marie Sklodowska-Curie Actions (MSCA) Individual Fellowship Grant for his ADMA5 project proposal.

HMAIED SHAIEK received the Engineering degree from the National Engineering School of Tunis, in 2002, the master's degree from the Université de Bretagne Occidentale, in 2003, and the Ph.D. degree from the Lab-STICC CNRS Team, Telecom Bretagne, in 2007. He was with Canon Inc., until 2009. He left the industry to integrate with the École Nationale d'Ingénieurs de Brest, as a Lecturer, from 2009 to 2010. In 2011, he joined the Conservatoire National des Arts et Métiers as an Associate Professor in electronics and signal processing. He holds three patents. He has authored or coauthored ten journal articles and over 35 conference papers. His research interests include performance analysis of multicarrier modulations with nonlinear power amplifiers, PAPR reduction, and power amplifier linearization. He contributed to the FP7 EMPHATIC European project and is involved in two national projects, such as Accent5 and Wong5, funded by the French National Research Agency.

DANIEL ROVIRAS was born in 1958. He received the Engineering degree from SUPÉLEC, Paris, France, in 1981, and the Ph.D. degree from the National Polytechnic Institute of Toulouse, Toulouse, France, in 1989. He spent in the industry as a Research Engineer for seven years. He joined the Electronics Laboratory, École Nationale Supérieure d'Électrotechnique, d'Électronique, d'Informatique, et des Télécommunications (ENSEEIHT). In 1992, he joined the Engineering School, ENSEEIHT, as an Assistant Professor, where he has been a Full Professor, since 1999. Since 2008, he has been a Professor with the Conservatoire National des Arts et Métiers (CNAM), Paris, where his teaching activities are related to radio-communication systems. He is currently a member of the CEDRIC Laboratory, CNAM. His research activity was first centered around transmission systems based on infrared links. Since 1992, his topics have been widened to more general communication systems, such as mobile and satellite communications systems, equalization, predistortion of nonlinear amplifiers, and multicarrier systems.